Front. Chem. Sci. Eng. 2023, 17(6): 716–725
https://doi.org/10.1007/s11705-022-2265-9

RESEARCH ARTICLE

Piezocatalytic performance of Fe_2O_3–Bi_2MoO_6 catalyst for dye degradation

Lili Cheng*, Xiaoyao Yu*, Danyao Huang, Hao Wang, Ying Wu (✉)

Key Laboratory of the Ministry of Education for Advanced Catalysis Materials, School of Chemistry and Materials Science, Zhejiang Normal University, Jinhua 321004, China

Abstract A Fe_2O_3–Bi_2MoO_6 heterojunction was synthesized via a hydrothermal method. Scanning electron microscopy, transmission electron microscopy, energy-dispersive X-ray, powder X-ray diffraction, Fourier transform infrared spectroscopy and ultra-violet–visible near-infrared spectrometry were performed to measure the structures, morphologies and optical properties of the as-prepared samples. The various factors that affected the piezocatalytic property of composite catalyst were studied. The highest rhodamine B degradation rate of 96.6% was attained on the 3% Fe_2O_3–Bi_2MoO_6 composite catalyst under 60 min of ultrasonic vibration. The good piezocatalytic activity was ascribed to the formation of a hierarchical flower-shaped microsphere structure and the heterostructure between Fe_2O_3 and Bi_2MoO_6, which effectively separated the ultrasound-induced electron–hole pairs and suppressed their recombination. Furthermore, a potential piezoelectric catalytic dye degradation mechanism of the Fe_2O_3–Bi_2MoO_6 catalyst was proposed based on the band potential and quenching effect of radical scavengers. The results demonstrated the potential of using Fe_2O_3–Bi_2MoO_6 nanocomposites in piezocatalytic applications.

Keywords piezocatalysis, Fe_2O_3–Bi_2MoO_6, dye decomposition, ultrasonic vibration

1 Introduction

With the rapid growth of industrialization, the issue of environmental water pollution has become increasingly severe [1]. Consequently, green approaches must be established to handle wastewater problems [2]. Notably, photocatalytic technology [3,4] can utilize abundant light energy to resolve the wastewater issue, and it has attracted much research attention. However, the low photogenerated charge separation efficiency under visible light and the inefficacy in the dark hinder the practical utilization of photocatalytic technology.

Therefore, an alternative method of dealing with dye wastewater problems must be explored. Similar to light and heat energy, mechanical energy is an extremely abundant energy resource [5]. Piezoelectric materials can convert mechanical vibration energy into electrical energy. The piezoelectric potential can induce the separation of charge carriers on the piezoelectric material surface, which can react with H_2O and O_2 to form active species. The formed species are adsorbed on the catalysts surface, consequently degrading the dye molecules. The whole process is called piezoelectric catalysis [6–8]. At present, piezoelectric catalytic technology is eliciting much attention and has achieved certain progress. Piezoelectric materials, including ZnO materials (nanorods, nanowires, and nanoparticles) [9–11], perovskite materials ($BaTiO_3$ and $SrTiO_3$) [12,13], 2D ultra-thin materials-sulfides (WS_2, CdS, and MoS_2) [14–16], and layered bismuth-based materials (BiOCl, Bi_2WO_6, $BiOIO_3$, $Bi_4Ti_3O_{12}$, $BiFeO_3$, and $Bi_{0.5}Na_{0.5}TiO_3$) [17–24], have attracted increasing interest.

Layered bismuth-based materials have been widely applied in the field of piezoelectricity. However, pure catalysts exhibit low piezoelectric catalytic performance due to their small specific surface area or low dielectric constant [25]. Therefore, many researchers have focused on improving piezoelectric catalytic performance by constructing special morphologies and heterojunctions [26–29]. The construction of heterojunctions facilitates the separation of electrons and holes, thereby enhancing the degradation efficiency of dyes. Singh et al. [30] reported that the degradation ratio of 5 $mg \cdot L^{-1}$ methylene blue (MB) solution over the $V_2O_5/BiVO_4$ composite catalyst can reach 80.0% under ultrasonic vibration for 240 min. Compared with the dye degradation

Received June 22, 2022; accepted September 25, 2022

E-mail: yingwu@zjnu.cn

* These authors contributed equally to this work.

performance of pure V_2O_5 and $BiVO_4$ particles, that of the V_2O_5/$BiVO_4$ heterojunction is enhanced by 22.0% and 13.0%, respectively. During the piezocatalytic reaction, the energy band of catalysts is bent, which is favorable for the transfer of free electrons and holes. The electrons can be transferred from the conduction band (CB) of $BiVO_4$ to that of V_2O_5, thus helping reduce the recombination of charge carriers and promoting piezoelectric catalytic activity. The construction of heterojunctions enhances the separation and utilization of piezoelectrically induced electron–hole pairs, thus enhancing the piezoelectric catalytic activity in rhodamine B (RhB) degradation. Similarly, Li et al. [31] prepared CoO/$BiFeO_3$ nanocomposites through the light deposition method. When ultrasonic vibration was applied for 90 min, the degradation ratio of the 10 ppm (10^{-6}) RhB solution was 82.0%.

The Bi_2MoO_6 catalyst can obtain special morphologies through simple preparation methods [32]. Owing to its intrinsic ferroelectricity [33], Bi_2MoO_6 is piezoelectric and can be used as a piezocatalyst. Cheng et al. [34] prepared HT-Bi_2MoO_6 microspheres via the hydrothermal method and evaluated their piezocatalytic performance. Although the microspheres exhibit an acceptable degradation performance at low RhB concentrations, only 22.2% of the RhB degradation ratio can be obtained at a concentration of 15 mg·L^{-1} under ultrasonic vibration for 45 min. According to these examples, the construction of heterostructures is an efficient means to enhance the piezocatalytic activity of bismuth-based materials. Accordingly, the piezocatalytic activity of Bi_2MoO_6 can also be improved by decorating it with a material with an appropriate band potential. Fe_2O_3 is a promising candidate material [35] because it is environmentally benign, inexpensive, and has a narrow energy band. Hence, Fe_2O_3 has been adopted in the field of photocatalytic degradation [36,37]. Chai et al. [38] studied a Fe_2O_3/PVDF-HFP porous film and degraded 50 mg·L^{-1} of TC solution via piezoelectric catalysis; they found that the addition of Fe_2O_3 can greatly improve the piezoelectric catalytic performance of PVDF-HFP porous films. However, the piezoelectric properties of Fe_2O_3 have rarely been studied, and no research has been conducted on the piezoelectric degradation of dyes by Fe_2O_3–Bi_2MoO_6 catalysts. The decoration of Fe_2O_3 on Bi_2MoO_6 could produce a type-II heterojunction and efficiently reduce the recombination of charge carriers, thereby facilitating the piezocatalytic reaction.

In this study, a Fe_2O_3–Bi_2MoO_6 heterojunction was synthesized through the hydrothermal method, and the effects of Fe_2O_3 content, catalytic reaction conditions, catalyst dosage, type and concentration of dyes, and ultrasonic machine power on the piezocatalytic property were investigated. In addition, the piezoelectric catalyst mechanism was inferred by combining the performance and characterization results.

2 Experimental

The Fe_2O_3–Bi_2MoO_6 composite catalysts were prepared by a hydrothermal method. The as-synthesized Fe_2O_3–Bi_2MoO_6 composite catalysts with different Fe_2O_3 contents were labeled as 1% Fe_2O_3–BM, 3% Fe_2O_3–BM and 5% Fe_2O_3–BM, and the pure Bi_2MoO_6 catalyst was denoted as BM.

The catalytic activity of the Fe_2O_3–BM catalyst was evaluated for the degradation of different dyes (50 mL of 15 mg·L^{-1} RhB, MB or methyl orange (MO) solution). In addition, the piezoelectric catalytic experiment was conducted in an ultrasonic cleaner (JP-020S) with a frequency of 40 kHz and power of 120 W.

The detailed information about the preparation and characterization of catalysts, piezocatalytic experiments, and free radical trapping experiment procedures is provided in the Electronic Supplementary Material (ESM).

3 Results and discussion

3.1 Catalyst characterization

The phase structures the Fe_2O_3–BM catalysts with different Fe_2O_3 contents were examined through X-ray diffraction (XRD). As shown in Fig. 1, the pristine BM catalyst showed apparent diffraction peaks at 2θ = 28.31°, 32.53°, 46.74°, 55.44°, which matched the (131), (200), (202), and (331) planes of orthogonal Bi_2MoO_6 (JCPDS 21-0102), respectively [32]. For the pure Fe_2O_3, obvious diffraction peaks were observed at 2θ = 24.14°, 33.01°, 35.97°, 40.35°, 49.41°, 54.04°, 62.29°, and 63.98° corresponding to (012), (125), (208), (128), (318), (324), (238), and (330) crystal planes, respectively, which are consistent with the characteristic peaks of Fe_2O_3 (JCPDS 33-0664). The XRD patterns of the Fe_2O_3–BM catalysts displayed only the characteristic peaks of BM without distinct Fe_2O_3 diffraction, which may be due to the small

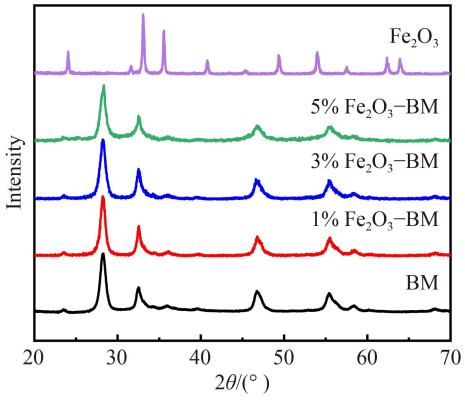

Fig. 1 X-ray diffraction patterns of the Fe_2O_3–BM catalysts.

amount of Fe_2O_3 and its uniform distribution on the BM surface.

The Fourier transform infrared (FTIR) spectra of the Fe_2O_3−BM catalysts with different Fe_2O_3 contents are presented in Fig. S1 (cf. ESM). For the pristine BM sample, the characteristic peaks at 542 and 723 cm^{-1} were attributed to Bi–O and Mo–O stretching vibrations, respectively [39], and the peaks at 3430, 1636 and 1380 cm^{-1} originated from O–H vibration [40]. The characteristic absorption peak of the Fe_2O_3−BM composite catalysts was almost identical to that of the pristine BM, indicating that the compounding of Fe_2O_3 had no effect on the structure of BM.

The morphology of the 3% Fe_2O_3−BM catalyst was analyzed via scanning electron microscopy (SEM) and transmission electron microscopy (TEM) (Fig. 2). As illustrated in Figs. 2(a)–2(c), the catalyst presented a flower-like microsphere structure composed of regular nanosheets. The morphology of the flower-like microsphere was also observed in the TEM photograph in Fig. 2(d), and the edges of the microspheres were rough. The microstructure of the catalyst was further examined through high-resolution TEM (HRTEM), and the results are shown in Figs. 2(e) and 2(f). Small nanoparticles were observed on the nanosheets with clear lattice fringes. The interplanar spacing of the nanosheets was 0.315 nm, which corresponded to the (131) plane of the BM catalyst, and the lattice fringe spacing on the nanoparticles is 0.276 nm, which belonged to the (104) crystal plane of the Fe_2O_3 catalyst [35–38]. The HRTEM results further proved that Fe_2O_3 nanoparticles were tightly loaded on the BM surfaces, indicating that the Fe_2O_3−BM composite catalysts were successfully prepared via the hydrothermal method. Moreover, the energy-dispersive spectroscopy (EDS) diagrams of the 3% Fe_2O_3−BM catalyst shown in Figs. 2(g)–2(j) implied that the elemental composition distributions of Bi, Mo, O and Fe elements in 3% Fe_2O_3−BM catalyst were similar, indicating that Fe_2O_3 was uniformly distributed on the BM surface. Although no information about Fe_2O_3 was observed in the XRD patterns and IR spectra, the HRTEM and EDS results clearly revealed the compound of Fe_2O_3 with BM.

The ultra-violet−visible spectroscopy (UV–Vis) absorption diffuse reflectance spectroscopy (DRS) spectra of the as-prepared catalysts are presented in Fig. 3. The absorption edges of the pristine BM and Fe_2O_3 were located at about 454 and 614 nm, respectively. The loading of Fe_2O_3 remarkably expanded the absorption region compared with the pristine BM. With the increase in Fe_2O_3 content, the absorption edge of the Fe_2O_3−BM catalysts exhibited red shift. According to the Tauc diagram, the band gaps of 1%, 3%, and 5% Fe_2O_3−BM is evaluated to be 2.67, 2.54 and 2.53 eV, respectively.

The elemental composition and chemical state of BM and the 3% Fe_2O_3−BM catalysts were characterized via X-ray photoelectron spectroscopy (XPS) (Fig. 4). The Bi 4f XPS spectra in Fig. 4(a) show two peaks at 159.2 and 164.4 eV, which are consistent with those of Bi $4f_{7/2}$ and Bi $4f_{5/2}$ [41]. In Fig. 4(b), the peaks located at around 232.5 and 235.6 eV originated from Mo $3d_{5/2}$ and Mo

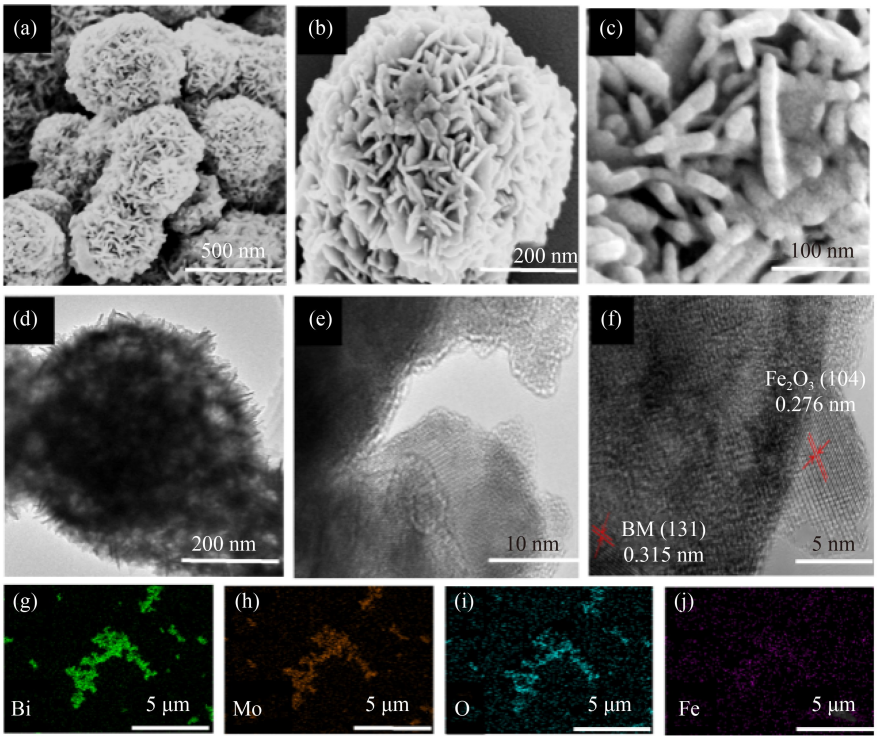

Fig. 2 SEM (a–c), TEM (d–f) images, and corresponding element mapping images (g–j) of 3% Fe_2O_3−BM catalyst.

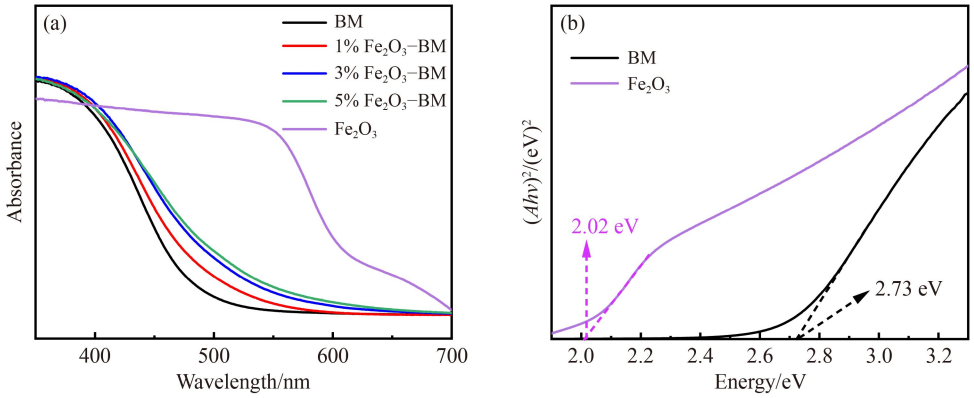

Fig. 3 (a) UV–Vis absorption spectra and (b) Tauc plots of different Fe_2O_3–BM catalysts.

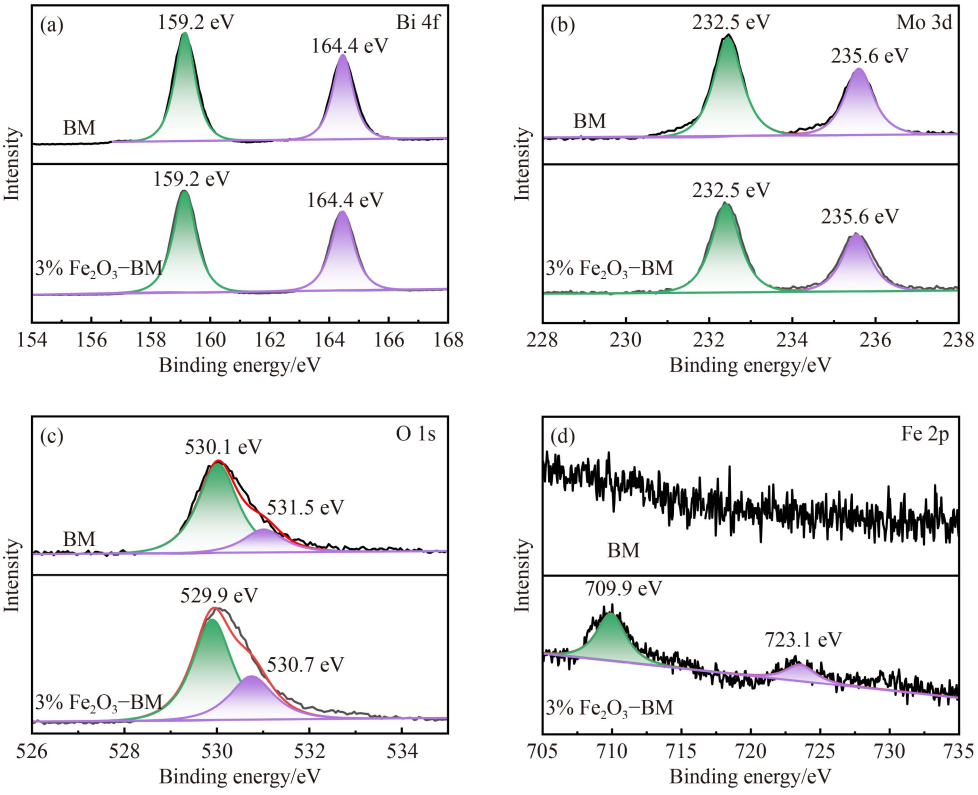

Fig. 4 XPS spectra of BM and Fe_2O_3–BM: (a) Bi 4f, (b) Mo 3d, (c) O 1s, (d) Fe 2p.

$3d_{3/2}$, respectively [42]. Figure 4(c) demonstrates that the O 1s spectra displayed peaks at 530.1 and 531.5 eV, which could be ascribed to the lattice oxygen and bridging hydroxyl species [43]. Compared with the O 1s binding energies of the pristine BM catalyst, those of the 3% Fe_2O_3–BM catalyst were reduced by 0.2 and 0.8 eV, which could be attributed to the fact that the tightly loaded Fe_2O_3 nanoparticles on the BM surface occupied part of the adsorption sites for hydroxyl species. In addition, the Fe $2p_{3/2}$ and Fe $2p_{1/2}$ peaks were located at 709.9 and 723.1 eV (Fig. 4(d)), indicating that the Fe element in the sample was in Fe^{3+} state [35].

Generally, the piezoelectric current response is effective evidence of charge separation. Therefore, a 390 s piezoelectric current response experiment was conducted on the pristine BM and different Fe_2O_3–BM catalysts by using ultrasonic machinery with vibration "on" and "off" cycle patterns. As shown in Fig. 5, the Fe_2O_3–BM catalysts exhibited higher piezocurrent than pristine Fe_2O_3 or BM, indicating that the introduction of Fe_2O_3 was beneficial to improving the piezoelectric catalytic performance. The 3% Fe_2O_3–BM catalyst showed the highest piezoelectric current response, suggesting its best free charge separation ability. However, 5% Fe_2O_3–BM showed a weak piezoelectric current response probably because that the excessive Fe_2O_3 content resulted in accumulation and a decrease in the contact interface, thus affecting the piezoelectric performance.

In addition, the dielectric constants of the Fe_2O_3−BM catalysts with different Fe_2O_3 contents were measured through electrochemical impedance spectroscopy (Fig. 6). Figure 6(a) indicates that arc radius of the 3% Fe_2O_3−BM catalyst was smaller than that of BM or Fe_2O_3, which meant it had better conductivity and smaller charge transfer resistance. Obviously, the added Fe_2O_3 facilitated the transfer and separation of the electron−hole pairs of BM by forming a heterojunction structure. As shown in Fig. 6(b), the 3% Fe_2O_3−BM composite had the lowest dielectric constant and was easily polarized.

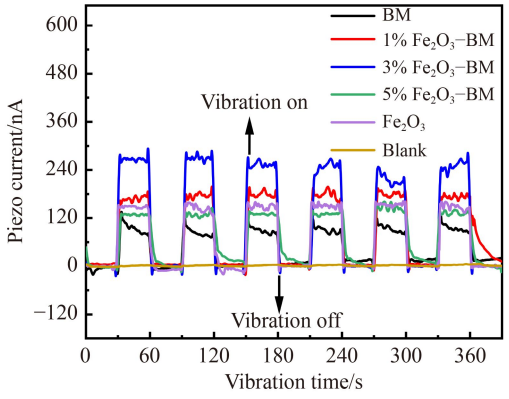

Fig. 5 Piezoelectric current response of different Fe_2O_3−BM catalysts

3.2 Piezoelectric catalytic performance

The piezocatalytic activities of the as-prepared catalysts were assessed by degrading RhB solution under ultrasonic vibration, and the results are given in Fig. 7. The RhB solution was hardly degraded without any piezocatalyst after vibrating for 60 min, indicating that the piezocatalyst played an extraordinary role in degrading dye. Compared with the piezoelectric activity of pristine BM, that of the Fe_2O_3−BM catalyst increased significantly due to the loading of Fe_2O_3. With the increase in Fe_2O_3 content, the degradation rate of the dye initially increased then decreased. The highest degradation percentage of 96.6% was achieved on the 3% Fe_2O_3−BM catalyst under ultrasonic vibration for 60 min. The RhB degradation ratio of 0.041 min^{-1} was 8.2 and 3.2 times higher than

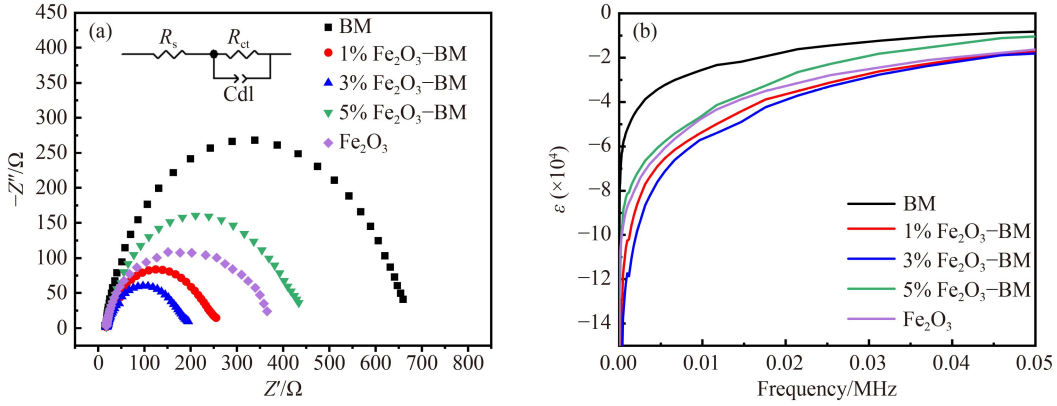

Fig. 6 (a) Electrochemical impedance spectra and (b) dielectric constants of different Fe_2O_3−BM catalysts.

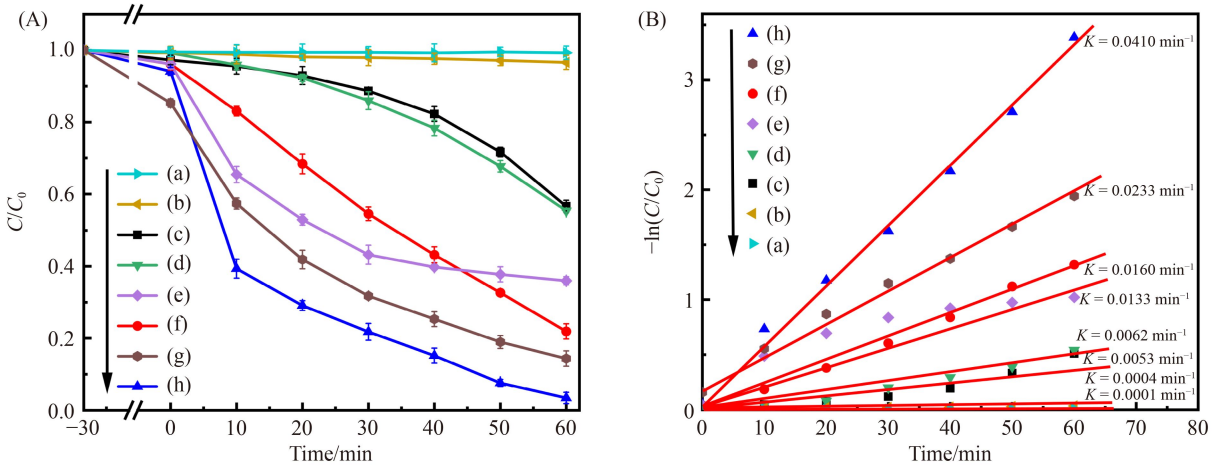

Fig. 7 (A) Piezoelectric activity of different catalysts and (B) the corresponding degradation rate: (a) without catalyst, (b) 3% Fe_2O_3−BM + mechanical stirring, (c) BM, (d) 5% Fe_2O_3−BM, (e) Fe_2O_3, (f) 1% Fe_2O_3−BM, (g) physical mixture of 3 wt % Fe_2O_3 and 97 wt % BM, (h) 3% Fe_2O_3−BM.

that of pristine BM and Fe_2O_3 catalyst, respectively. In comparison, the physical mixture (3 wt % Fe_2O_3 + 97 wt % BM) showed lower activity (85.7%), suggesting that the close contact between Fe_2O_3 and BM contributed to the enhancement of piezocatalytic performance [44].

However, the 3% Fe_2O_3−BM catalyst exhibited negligible piezocatalytic activity in the absence of vibration, revealing that ultrasonic vibration was crucial for dye decomposition. The piezoelectric material BM was deformed by ultrasonic vibration, which helped induce the catalyst to generate free charged electrons and holes. Under the action of mechanical stress, the free electrons and holes generated a piezoelectric potential, which attracted the heat-excited free charges in the BM catalyst towards the opposite directions of the crystal surfaces. The separated free electrons and holes accumulated at the interface and reacted with O_2 to generate active species to degrade the dye molecules. The loaded Fe_2O_3 could capture free charges on the BM surface, further promoting charge separation. An appropriate Fe_2O_3 content was determined to be conducive to the separation of free charges, whereas an excessive Fe_2O_3 content resulted in accumulation and a decrease in the contact interface.

Figure 8 showed the effect of catalyst amount, RhB concentration, and power on the piezoelectric catalytic degradation performance. The effect of the 3% Fe_2O_3−BM catalyst amount on the piezoelectric decomposition of the RhB solution is presented in Figs. 8(a) and 8(b). With the increase in catalyst amount, the piezoelectric catalytic performance improved to a certain degree. When the catalyst amount increased to 10 mg, the piezoelectric catalytic degradation ratio could reach 96.6%. Owing to the increase in the catalyst amount, more active sites were supplied for the reaction, thereby stimulating the degradation of the dye molecules. Further increasing the amount of the catalyst, however, led to a decrease in piezoelectric catalytic efficiency down to 87.5%, which could be attributed to the fact that too much catalyst increases the collision frequency and in turn gives rise to the recombination of free charges on the catalyst surface. Consequently, the active species are correspondingly reduced, and the piezoelectric catalytic efficiency decreases.

Figures 8(c) and 8(d) reveal the effect of dye concentration on the decomposition property of piezoelectric catalyst. When the concentration of the RhB solution increased from 5 to 15 mg·L^{-1}, the decomposition rate slightly decreased. When the concentration of the RhB solution increased to 20 mg·L^{-1}, only 19.3% of the degradation ratio was obtained after 60 min. Excessive dye concentration led to a decrease in piezoelectric catalytic performance, which may be due to the large amount of dye molecules adsorbed on the catalyst surface covering the active sites on the catalysts surface, therefore reducing the piezoelectric catalytic performance.

The influence of power on the piezoelectric catalytic property is presented in Figs. 8(e) and 8(f). With the enhancement of ultrasonic power, the piezoelectric catalytic performance was considerably enhanced because increasing the ultrasonic power resulted in increased stress, thus causing the catalyst to deform to a greater degree and producing more free electrons and holes. A strong piezoelectric potential is conducive to the separation of free charges, which react with O_2 and H_2O to produce numerous active species, hence accelerating the rapid decomposition of dye molecules.

The stability and repeatability of the 3% Fe_2O_3−BM catalyst were evaluated through piezocatalytic decomposition RhB cycle experiments. For each cycle experiment, the catalyst was recovered by centrifugation, washed with distilled water and ethanol, dried in a vacuum, and reused for the degradation of fresh dye solution. As demonstrated in Fig. S2 (cf. ESM), after four cycles, the catalytic activity did not decrease considerably, indicating that the 3% Fe_2O_3−BM catalyst had good durability and repeatability.

Figure S3 (cf. ESM) presents the time-dependent absorption spectra of RhB, MB and MO solutions in the presence of the 3% Fe_2O_3−BM catalyst and its piezoelectric catalytic degradation activity. The color of the three dye solutions gradually lightened under ultrasonic vibration for 60 min. The 3% Fe_2O_3−BM catalyst exhibited excellent piezoelectric catalytic performance of 96.6%, 96.5% and 92.4% in the decomposition of 15 mg·L^{-1} RhB, MB and MO dyes, respectively.

3.3 Possible piezoelectric catalytic mechanism

The active species during the piezoelectric decomposition process were determined through free radical trapping experiments. Figure 9 shows that the addition of scavengers retarded the piezocatalytic reaction, revealing that the reactive species were conducive to the piezocatalytic reaction. The inhibitory effect on RhB degradation followed the order of triethanolamine (TEA) > benzoquinone (BQ) > isopropyl alcohol (IPA), which meant that the significance of the reactive species in the piezocatalytic reaction was in the order of $h^+ > \cdot O_2^- > \cdot OH$.

A possible piezoelectric catalytic mechanism of the Fe_2O_3−BM composite catalyst for degrading RhB solution was speculated based on the above-mentioned results, as presented in Fig. 10. Under ultrasonic vibration, the cavitation effect induced a high-frequency mechanical shock on the catalyst and triggered the generation of a built-in electric field [45,46], which was conducive to the production of abundant electrons and holes on the catalyst surface. Under the action of the piezoelectric potential, the thermally excited free charges accumulated on the piezocatalyst surface and reacted with hydroxyl or dissolved oxygen to form reactive species, which then induced the surface piezocatalytic degradation of dye molecules. In addition, some researchers deem that the "hot spot" produced by the ultrasonic cavitation effect in

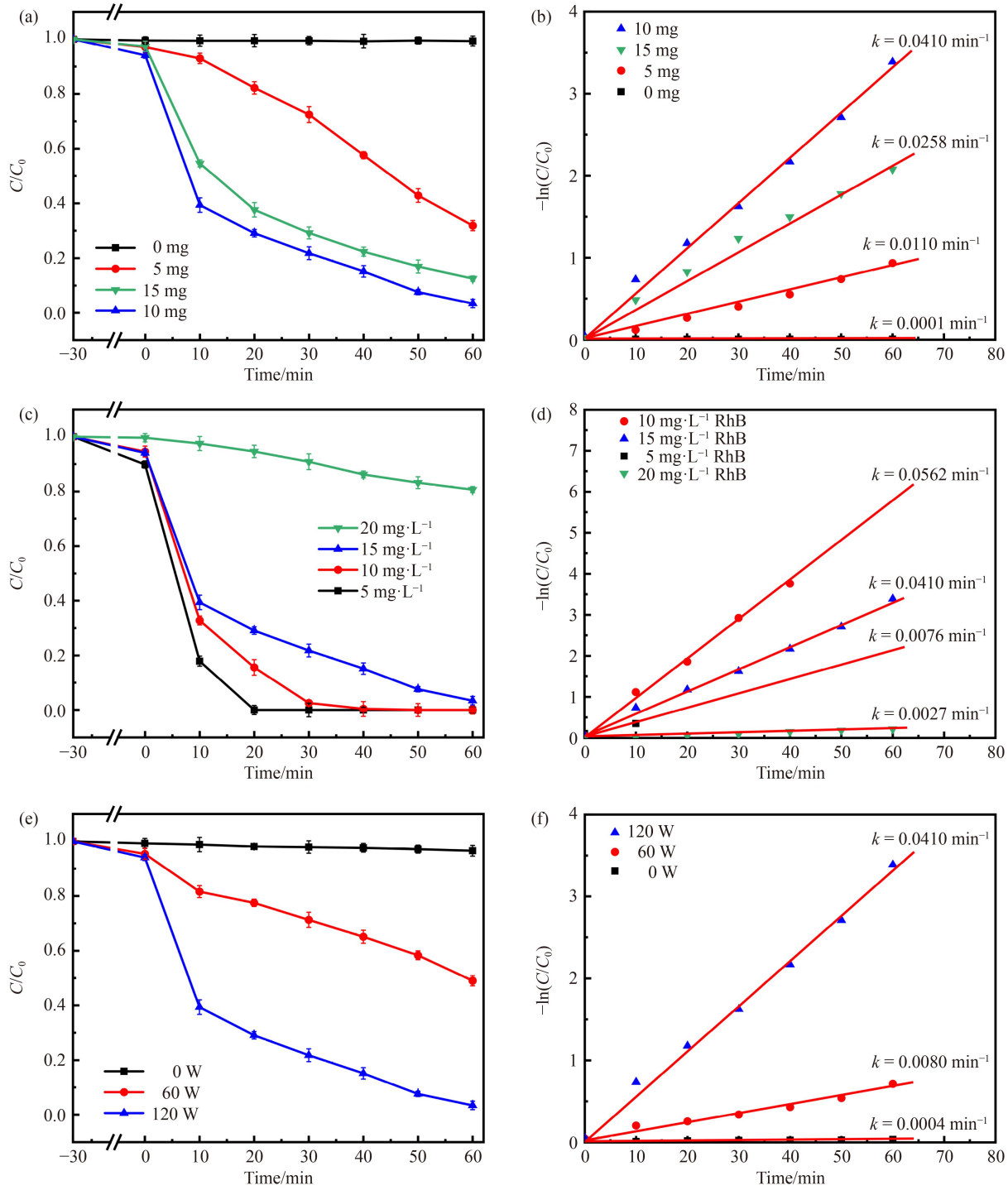

Fig. 8 Effect of (a, b) 3% Fe_2O_3–BM catalyst amount, (c, d) RhB concentration, (e, f) power on the piezoelectric catalytic degradation performance.

a water medium can reach a very high temperature (about 5000 °C) [47]. The catalyst can generate free charges under such a high temperature, which then migrate to the surface and facilitate the formation of active species [48,49]. However, regardless of where the free charges come from, the composite of Bi_2MoO_6 and Fe_2O_3 undoubtedly promotes the separation of electrons and holes. In the current study, the CB and valence band (VB) potentials of Bi_2MoO_6 and Fe_2O_3 were calculated based on Mulliken electro-negativity, and further determined by valence-band X-ray photoelectron spectroscopy spectroscopy (VB-XPS). The results are described in Fig. S4 (cf. ESM). Given that the CB position of Fe_2O_3 is higher than that of BM, free electrons tended to

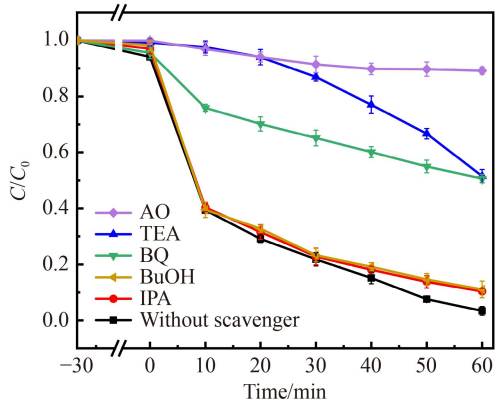

Fig. 9 Active species capture experiment of 3% Fe_2O_3–BM.

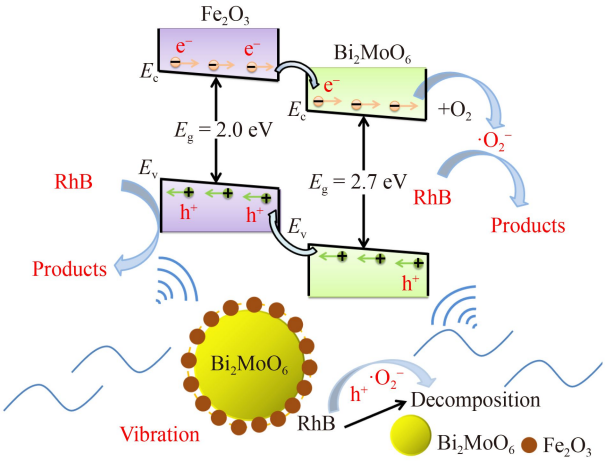

Fig. 10 Piezoelectric catalytic mechanism diagram of 3% Fe_2O_3–BM catalyst.

accumulate on the CB side of BM. On the other hand, the VB position of Fe_2O_3 is lower than that of BM, so holes tend to accumulate on the Fe_2O_3 VB side. Therefore, the matched band structure of Fe_2O_3 and BM facilitated the separation and utilization of piezoelectric-induced charge carriers. The VB value of the as-prepared Fe_2O_3 catalysts was 1.30 eV, which is lower than E_0 ($\cdot OH/OH^-$ = 2.38 eV) [50], indicating that the holes could not easily react with OH^-/H_2O to form $\cdot OH$. Consequently, a large quantity of holes accumulated on the VB side of Fe_2O_3 and directly degraded the dye molecules [35]. At the same time, these free electrons reacted with O_2 to form $\cdot O_2^-$ active species, which were adsorbed on the catalyst surface and further degraded the dye molecules. The main reaction routes of piezoelectric catalysis of the Fe_2O_3–BM composite catalysts are as follows:

$$Fe_2O_3 - BM \rightarrow Fe_2O_3 - BM(e^- + h^+) \quad (1)$$

$$O_2 + e^- \rightarrow \cdot O_2^- \quad (2)$$

$$\cdot O_2^-(\text{or } h^+) + \text{dye} \rightarrow \text{decomposition} \quad (3)$$

4 Conclusions

In this work, the Fe_2O_3–BM composite catalyst synthesized via a hydrothermal method showed a better piezocatalytic property for the degradation of RhB compared with pure Fe_2O_3 or BM. The improvement was attributed to its flower-shaped microsphere structure composed of nanosheets, which facilitated the generation of a strong piezoelectric field under ultrasonic vibration and the separation of free charges on the material surface. The free electrons reacted with the dissolved O_2 in the water to form active species with a strong oxidizing ability and these species were adsorbed on the catalyst surface, thereby further degrading the dye molecules at a staggering rate. This research provides a promising piezocatalyst and encourages further research on the rational utilization of abundant mechanical energy to treat dye wastewater and improvement of piezocatalytic material activity by constructing heterostructures.

Acknowledgements This work was supported by the National Natural Science Foundation of China (Grant No. 22272151) and Natural Science Foundation of Zhejiang Province (Grant No. LY16B030002).

Electronic Supplementary Material Supplementary material is available in the online version of this article at https://dx.doi.org/10.1007/s11705-022-2265-9 and is accessible for authorized users.

References

1. Xia Y T, Jia Y M, Qian W Q, Xu X L, Wu Z, Han Z C, Hong Y T, You H L, Ismail M, Bai G, Wang L. Pyroelectrically induced pyro-electro-chemical catalytic activity of $BaTiO_3$ nanofibers under room-temperature cold-hot cycle excitations. Metals, 2017, 7(4): 122
2. Jing L Q, Xie M, Xu Y G, Tong C, Zhao H, Zhong N, Li H M, Gates I D, Hu J G. Multifunctional 3D $MoS_x/Zn_3In_2S_6$ nanoflower for selective photothermal-catalytic biomass oxidative and non-selective organic pollutants degradation. Applied Catalysis B: Environmental, 2022, 318: 121814
3. Wang R, Liu J Y, Wang B, Yang R Z, Zhu S M, Song Y H, Hua Y J, Yan J, Cheng M, Xu H, Li H. Noble-metal-free Co-N-graphene/PDI for significant enhancement of photocatalytic performance. Journal of Alloys and Compounds, 2022, 925: 166370
4. Pang Z Y, Wang B, Yan X W, Wang C T, Yin S, Li H M, Xia J X. $CdBiO_2Br$ nanosheets in situ strong coupling to carbonized polymer dots and improved photocatalytic activity for organic pollutants degradation. Chinese Chemical Letters, 2022, 33(12): 5189–5195
5. Peng M Z, Liu Y D, Yu A F, Zhang Y, Liu C H, Liu J Y, Wu W, Zhang K, Shi X Q, Kou J Z, Zhai J, Wang Z L. Flexible self-powered GaN ultraviolet photoswitch with piezo-phototronic effect enhanced on/off ratio. ACS Nano, 2016, 10(1): 1572–1579
6. Chen L, Zhang W Q, Wang J F, Li X J, Li Y, Hu X, Zhao L H,

Wu Y, He Y M. High piezo/photocatalytic efficiency of Ag/Bi_5O_7I nanocomposite using mechanical and solar energy for N_2 fixation and methyl orange degradation. Green Energy & Environment, 2023, 8(1): 283–295

7. Wang L K, Wang J F, Ye C Y, Wang K Q, Zhao C R, Wu Y, He Y M. Photodeposition of CoO_x nanoparticles on $BiFeO_3$ nanodisk for efficiently piezocatalytic degradation of rhodamine B by utilizing ultrasonic vibration energy. Ultrasonics Sonochemistry, 2021, 80: 105813
8. Zheng S, Li X J, Zhang J Y, Wang J F, Zhao C R, Hu X, Wu Y, He Y. One-step preparation of MoO_x/ZnS/ZnO composite and its excellent performance in piezocatalytic degradation of Rhodamine B under ultrasonic vibration. Journal of Environmental Sciences, 2023, 125: 1–13
9. Xu X L, Jia Y M, Xiao L B, Wu Z. Strong vibration-catalysis of ZnO nanorods for dye wastewater decolorization via piezo-electro-chemical coupling. Chemosphere, 2018, 193: 1143–1148
10. Ou C, Sanchez-Jimenez P E, Datta A, Boughey F L, Whiter R A, Sahonta S L, Kar-Narayan S. Template-assisted hydrothermal growth of aligned Zinc Oxide nanowires for piezoelectric energy harvesting applications. ACS Applied Materials & Interfaces, 2016, 8(22): 13678–13683
11. Ning X E, Hao A Z, Cao Y L, Hu J D, Xie J, Jia D Z. Effective promoting piezocatalytic property of zinc oxide for degradation of organic pollutants and insight into piezocatalytic mechanism. Journal of Colloid and Interface Science, 2020, 577: 290–299
12. Xu X L, Wu Z, Xiao L B, Jia Y M, Ma J P, Wang F F, Wang L, Wang M S, Huang H T. Strong piezo-electro-chemical effect of piezoelectric $BaTiO_3$ nanofibers for vibration-catalysis. Journal of Alloys and Compounds, 2018, 762: 915–921
13. Ling J S, Wang K, Wang Z Y, Huang H T, Zhang G K. Enhanced piezoelectric-induced catalysis of $SrTiO_3$ nanocrystal with well-defined facets under ultrasonic vibration. Ultrasonics Sonochemistry, 2020, 61: 104819
14. Cao R M, Wu R, Zhang D, Xu S. Ultrahigh degradation efficiency of AB Type in-plane reverse polarization WS_2 nano sheets in dark by piezo-catalyst effect. Applied Surface Science, 2021, 553: 149557
15. Abbood H A, Alabadi A, Al-Hawash A B, Abbood A A, Huang K X. Square CdS micro/nanosheets as efficient photo/piezo-bi-catalyst for hydrogen production. Catalysis Letters, 2020, 150(11): 3059–3070
16. Wu J M, Sun Y G, Chang W E, Lee J T. Piezoelectricity induced water splitting and formation of hydroxyl radical from active edge sites of MoS_2 nanoflowers. Nano Energy, 2018, 46: 372–382
17. Shao D K, Zhang L, Sun S M, Wang W Z. Oxygen reduction reaction for generating H_2O_2 through a piezo-catalytic process over bismuth oxychloride. ChemSusChem, 2018, 11(3): 527–531
18. Xu X L, Xiao L B, Wu Z, Jia Y M, Ye X, Wang F F, Yuan B, Yu Y, Huang H T, Zou G F. Harvesting vibration energy to piezo-catalytically generate hydrogen through Bi_2WO_6 layered-perovskite. Nano Energy, 2020, 78: 105351
19. Chen J Y, Lei H, Ji S L, Wu M X, Zhou B C, Dong X P. Synergistic catalysis of $BiOIO_3$ catalyst for elimination of organic pollutants under simultaneous photo-irradiation and ultrasound-vibration treatment. Journal of Colloid and Interface Science, 2021, 601: 704–713
20. Tu S C, Huang H W, Zhang T R, Zhang Y H. Controllable synthesis of multi-responsive ferroelectric layered perovskite-like $Bi_4Ti_3O_{12}$: photocatalysis and piezoelectric-catalysis and mechanism insight. Applied Catalysis B: Environmental, 2017, 219: 550–562
21. Wu J, Qin N, Lin E Z, Yuan B W, Kang Z H, Bao D H. Synthesis of $Bi_4Ti_3O_{12}$ decussated nanoplates with enhanced piezocatalytic activity. Nanoscale, 2019, 11(44): 21128–21136
22. You H L, Wu Z, Zhang L H, Ying Y R, Liu Y, Fei L F, Chen X X, Jia Y M, Wang Y J, Wang F F, Ju S, Qiao J, Lam C H, Huang H. Harvesting the vibration energy of $BiFeO_3$ nanosheets for hydrogen evolution. Angewandte Chemie International Edition, 2019, 58(34): 11779–11784
23. Mushtaq F, Chen X Z, Hoop M, Torlakcik H, Pellicer E, Sort J, Gattinoni C, Nelson B J, Pané S. Piezoelectrically enhanced photocatalysis with $BiFeO_3$ nanostructures for efficient water remediation. iScience, 2018, 4: 236–246
24. Zhou X F, Sun Q W, Zhai D, Xue G L, Luo H, Zhang D. Excellent catalytic performance of molten-salt-synthesized $Bi_{0.5}Na_{0.5}TiO_3$ nanorods by the piezo-phototronic coupling effect. Nano Energy, 2021, 84: 105936
25. Zhang L W, Xu T G, Zhao X, Zhu Y F. Controllable synthesis of Bi_2MoO_6 and effect of morphology and variation in local structure on photocatalytic activities. Applied Catalysis B: Environmental, 2010, 98(3-4): 138–146
26. Chen L, Dai X Q, Li X J, Wang J F, Chen H F, Hu X, Lin H J, He Y M, Wu Y, Fan M. A novel $Bi_2S_3/KTa_{0.75}Nb_{0.25}O_3$ nanocomposite with high efficiency for photocatalytic and piezocatalytic N_2 fixation. Journal of Materials Chemistry A: Materials for Energy and Sustainability, 2021, 9(22): 13344–13354
27. Dai X Q, Chen L, Li Z Y, Li X J, Wang J F, Hu X, Zhao L H, Jia Y M, Sun S X, Wu Y, He Y. $CuS/KTa_{0.75}Nb_{0.25}O_3$ nanocomposite utilizing solar and mechanical energy for catalytic N_2 fixation. Journal of Colloid and Interface Science, 2021, 603: 220–232
28. Chen L, Wang J F, Li X J, Zhang J Y, Zhao C R, Hu X, Lin H J, Zhao L H, Wu Y, He Y M. Facile preparation of $Ag_2S/KTa_{0.5}Nb_{0.5}O_3$ heterojunction for enhanced performance in catalytic nitrogen fixation via photocatalysis and piezo-photocatalysis. Green Energy & Environment, 2022, in press
29. Li X J, Wang J F, Zhang J Y, Zhao C R, Wu Y, He Y M. Cadmium sulfide modified zinc oxide heterojunction harvesting ultrasonic mechanical energy for efficient decomposition of dye wastewater. Journal of Colloid and Interface Science, 2022, 607: 412–422
30. Singh G, Kumar M, Vaish R. Promising multicatalytic and adsorption capabilities in $V_2O_5/BiVO_4$ composite pellets for water-cleaning application. Surfaces and Interfaces, 2021, 23: 100924
31. Li Y, Chen H F, Wang L K, Wu T T, Wu Y, He Y M. $KNbO_3$/ZnO heterojunction harvesting ultrasonic mechanical energy and solar energy to efficiently degrade methyl orange. Ultrasonics Sonochemistry, 2021, 78: 105754
32. Zhang X C, Ren G M, Zhang C M, Li R, Zhao Q, Fan C M.

Photocatalytic reduction of CO_2 to CO over 3D Bi_2MoO_6 microspheres: simple synthesis, high efficiency and selectivity, reaction mechanism. Catalysis Letters, 2020, 150(9): 2510–2516

33. Benedek N A, Rondinelli J M, Djani H, Ghosez P, Lightfoot P. Understanding ferroelectricity in layered perovskites: new ideas and insights from theory and experiments. Dalton Transactions, 2015, 44(23): 10543–10558
34. Cheng L L, Huang D Y, Zhang Y, Wu Y. Preparation and piezoelectric catalytic performance of HT-Bi_2MoO_6 microspheres for dye degradation. Advanced Powder Technology, 2021, 32(9): 3346–3354
35. Zhao J, Lu Q F, Wei M Z, Wang C Q. Synthesis of one-dimensional α-Fe_2O_3/Bi_2MoO_6 heterostructures by electrospinning process with enhanced photocatalytic activity. Journal of Alloys and Compounds, 2015, 646: 417–424
36. Li S J, Hu S W, Zhang J L, Jiang W, Liu J S. Facile synthesis of Fe_2O_3 nanoparticles anchored on Bi_2MoO_6 microflowers with improved visible light photocatalytic activity. Journal of Colloid and Interface Science, 2017, 497: 93–101
37. Wang W L, Zhao W L, Huang H M, Chen R Y, Shi H F. A 2D/2D S-scheme photo-Fenton catalyst based on ultrathin Bi_2MoO_6 and Fe_2O_3 hexagonal nanosheets for efficient tetracycline degradation. Catalysis Science & Technology, 2021, 11(8): 2948–2956
38. Chai M N, Tong W S, Wang Z H, Chen Z S, An Y C, Zhang Y H. Piezoelectric-Fenton degradation and mechanism study of Fe_2O_3/PVDF-HFP porous film drove by flowing water. Journal of Hazardous Materials, 2022, 430: 128446
39. Xiao K, Huang H W, Tian N, Zhang Y H. Mixed-calcination synthesis of Bi_2MoO_6/g-C_3N_4 heterojunction with enhanced visible-light-responsive photoreactivity for RhB degradation and photocurrent generation. Materials Research Bulletin, 2016, 83: 172–178
40. Zhang M Y, Shao C L, Zhang P, Su C Y, Zhang X, Liang P P, Sun Y Y, Liu Y C. Bi_2MoO_6 microtubes: Controlled fabrication by using electrospun polyacrylonitrile microfibers as template and their enhanced visible light photocatalytic activity. Journal of Hazardous Materials, 2012, 225-226: 155–163
41. Cai J S, Huang J Y, Lai Y K. Correction: 3D Au-decorated Bi_2MoO_6 nanosheet/TiO_2 nanotube array heterostructure with enhanced UV and visible-light photocatalytic activity. Journal of Materials Chemistry A: Materials for Energy and Sustainability, 2017, 5(31): 16422
42. Tao R, Shao C L, Li X H, Li X W, Liu S, Yang S, Zhao C C, Liu Y C. Bi_2MoO_6/$BiFeO_3$ heterojunction nanofibers: enhanced photocatalytic activity, charge separation mechanism and magnetic separability. Journal of Colloid and Interface Science, 2018, 529: 404–414
43. Zheng Y Q, Jia Y M, Li H M, Wu Z, Dong X P. Enhanced piezo-electro-chemical coupling of $BaTiO_3$/g-C_3N_4 nanocomposite for vibration-catalysis. Journal of Materials Science, 2020, 55(1): 14787–14797
44. Shi J L. On the synergetic catalytic effect in heterogeneous nanocomposite catalysts. Chemical Reviews, 2013, 113(3): 2139–2181
45. Zhang A, Liu Z Y, Xie B, Lu J S, Guo K, Ke S M, Shu L L, Fan H Q. Vibration catalysis of eco-friendly $Na_{0.5}K_{0.5}NbO_3$-based piezoelectric: an efficient phase boundary catalyst. Applied Catalysis B: Environmental, 2020, 279: 119353
46. Shi J D, Zeng W, Dai Z H, Wang L, Wang Q, Lin S P, Xiong Y, Yang S, Shang S M, Chen W, Zhao L, Ding X, Tao X, Chai Y. Piezocatalytic foam for highly efficient degradation of aqueous organics. Small Science, 2021, 1(2): 2000011
47. Wang Y F, Zhao D, Ji H W, Liu G L, Chen C C, Ma W H, Zhu H Y, Zhao J C. Sonochemical hydrogen production efficiently catalyzed by Au/TiO_2. Journal of Physical Chemistry C, 2010, 114(41): 17728–17733
48. Feng Y W, Ling L L, Wang Y X, Xu Z M, Cao F L, Li H X, Bian Z F. Engineering spherical lead zirconate titanate to explore the essence of piezo-catalysis. Nano Energy, 2017, 40: 481–486
49. Wang J, Ma T, Zhang Z H, Zhang X D, Jiang Y F, Pan Z J, Wen F Y, Kang P L, Zhang P. Investigation on the sonocatalytic degradation of methyl orange in the presence of nanometer anatase and rutile TiO_2 powders and comparison of their sonocatalytic activities. Desalination, 2006, 195(1-3): 294–305
50. Li S J, Zhang L S, Wang H L, Chen Z G, Hu J Q, Xu K B, Liu J S. Ta_3N_5-Pt nonwoven cloth with hierarchical nanopores as efficient and easily recyclable macroscale photocatalysts. Scientific Reports, 2014, 4(1): 3978